1521-009X/50/1/58–64$35.00
Drug Metabolism and Disposition

https://doi.org/10.1124/dmd.121.000546
Drug Metab Dispos 50:58–64, January 2022

New Pharmacokinetic Parameters of Imaging Substrates Quantified from Rat Liver Compartments

Catherine M. Pastor and Kim L.R. Brouwer

Department of Radiology, University Hospital of Geneva, Switzerland (C.M.P.); Université de Paris, Centre de recherche sur l'inflammation, Inserm, U1149, CNRS, ERL8252, F-75006 Paris, France (C.M.P.); and Division of Pharmacotherapy and Experimental Therapeutics, UNC Eshelman School of Pharmacy, University of North Carolina, Chapel Hill, North Carolina (K.L.R.B.)

Received May 18, 2021; accepted October 18, 2021

ABSTRACT

Hepatobiliary imaging is increasingly used by pharmacologists to quantify liver concentrations of transporter-dependent drugs. However, liver imaging does not quantify concentrations in extracellular space, hepatocytes, and bile canaliculi. Our study compared the compartmental distribution of two hepatobiliary substrates gadobenate dimeglumine [BOPTA; 0.08 liver extraction ratio (ER)] and mebrofenin (MEB; 0.93 ER) in a model of perfused rat liver. A gamma counter placed over livers measured liver concentrations. Livers were preperfused with gadopentetate dimeglumine to measure extracellular concentrations. Concentrations coming from bile canaliculi and hepatocytes were calculated. Transporter activities were assessed by concentration ratios between compartments and pharmacokinetic parameters that describe the accumulation and decay profiles of hepatocyte concentrations. The high liver concentrations of MEB relied mainly on hepatocyte and bile canaliculi concentrations. In contrast, the three compartments contributed to the low liver concentrations obtained during BOPTA perfusion. Nonlinear regression analysis of substrate accumulation in hepatocytes revealed that cellular efflux is measurable ~4 minutes after the start of perfusion. The hepatocyte-to-extracellular concentration ratio measured at this time point was much higher during MEB perfusion. BOPTA transport by multidrug resistance associated protein 2 induced an aquaporin-mediated water transport, whereas MEB transport did not. BOPTA clearance from hepatocytes to bile canaliculi was higher than MEB clearance. MEB did not efflux back to sinusoids, whereas BOPTA basolateral efflux contributed to the decrease in hepatocyte concentrations. In conclusion, our ex vivo model quantifies substrate compartmental distribution and transport across hepatocyte membranes and provides an additional understanding of substrate distribution in the liver.

SIGNIFICANCE STATEMENT

When transporter-dependent drugs target hepatocytes, cellular concentrations are important to investigate. Low concentrations on cellular targets impair drug therapeutic effects, whereas excessive hepatocyte concentrations may induce cellular toxicity. With a gamma counter placed over rat perfused livers, we measured substrate concentrations in the extracellular space, hepatocytes, and bile canaliculi. Transport across hepatocyte membranes was calculated. The study provides an additional understanding of substrate distribution in the liver.

Introduction

Over previous decades, the drug plasma concentration decay has been extensively studied. In the meantime, models to estimate drug hepatic clearance (CL_H) are still debated by experts (Benet et al., 2018; Rostami-Hodjegan, 2018; Rowland and Pang, 2018). However, when transporter-dependent drugs target hepatocytes, cellular concentrations are as important as systemic concentrations to investigate (Zhang et al., 2019). Low concentrations on cellular targets impair drug therapeutic effects, whereas excessive hepatocyte concentrations may induce cellular toxicity (Guo et al., 2018; Beaudoin et al., 2021). Membrane transporters determine hepatocyte concentrations of numerous drugs and endogenous substrates and create asymmetric distributions between liver and plasma (Riccardi et al., 2017; Guo et al., 2018; Zhang et al., 2019). Consequently, hepatobiliary imaging is increasingly used by pharmacologists to quantify the distribution of transporter-dependent drugs.

Several research groups took advantage of liver imaging to assess liver concentrations of hepatobiliary substrates (contrast agents and tracers)

This work was supported by the Swiss National Foundation [Grant 310030-126030].
dx.doi.org/10.1124/dmd.121.000546.

ABBREVIATIONS: BOPTA, gadobenate dimeglumine; C_{BC}, concentration in bile canaliculi measured by the counter; C_{bile}, in situ concentration in bile duct and bile canaliculi; C_{EC}, extracellular concentration; C_{ef}, concentrations that efflux back into sinusoids (rinse period); C_{HC}, hepatocyte concentration; $C_{HC,78\%}$, hepatocyte concentration measured by the counter; $C_{HC100\%}$, in situ concentration in hepatocytes; C_{in}, concentration in portal vein; CL_{bile}, clearance from hepatocytes to bile canaliculi; CL_{ef}, clearance from hepatocytes back to sinusoids; CL_H, hepatic clearance; CL_{in}, hepatocyte influx clearance; C_{liver}, liver concentration; C_{out}, concentration in hepatic veins; DTPA, gadopentetate dimeglumine; ER, extraction ratio; $k_{fast,HC}$, fast elimination rate constant of hepatocyte concentration; KHB, Krebs-Henseleit-bicarbonate; $k_{slow,HC}$, slow elimination rate constant of hepatocyte concentration; MEB, mebrofenin; Mrp2, multidrug resistance associated protein 2; Mrp3, multidrug resistance associated protein 3; Oatp, organic anion transporting polypeptide; PRL, perfused rat liver; Q_{bile}, bile flow rate; Q_H, liver flow rate; $R_{bile/EC}$, concentration ratio of bile canaliculi and extracellular space; $R_{bile/HC}$, concentration ratio of bile canaliculi and hepatocytes; $R_{HC/EC}$, concentration ratio of hepatocytes and extracellular space; $R_{HV/HC}$, concentration ratio of hepatic veins and hepatocytes (rinse); T_0, time when hepatocyte efflux affects C_{HC}; v, removal rate from sinusoid; v_{bile}, bile excretion rate; v_{ef}, basolateral efflux rate from hepatocytes back to sinusoids; v_{in}, hepatocyte influx rate.

and estimate rodent and human transporter function (Ali et al., 2018; Guo et al., 2018; Leporq et al., 2018; Tournier et al., 2018; Billington et al., 2019; De Lombaerde et al., 2019; Hernandez Lozano et al., 2019; Hernandez Lozano and Langer, 2020). Pharmacokinetic modeling is applied to analyze liver images and calculate clearances mediated by hepatocyte transporters.

However, these studies rely on liver concentrations but do not quantify concentrations in extracellular space, hepatocytes, and bile canaliculi (Fig. 1C). Substrate diffusion from sinusoids governs the extracellular concentrations, which can be quantified during the perfusion of extracellular substrates such as gadopentetate dimeglumine (DTPA) (Pastor et al., 2003). In normal rats, hepatocyte concentrations contribute largely to liver concentrations, and their volume represents 78% of liver weight (Blouin et al., 1977). In contrast, concentrations in bile canaliculi are typically high, but the canalicular volume represents only 0.43% of liver weight. In liver regions of interest, magnetic resonance imaging, single photon emission computed tomography, and positron emission tomography systems detect from each compartment the in situ concentrations corrected by the volume ratio between compartment and liver. The sum of these concentrations are the liver concentrations (Sourbron, 2014). The Sourbron review clearly explains the difference between in situ substrate concentrations in liver compartments and concentrations measured by an imaging system.

Previous publications used pharmacokinetic modeling to describe the basolateral and canalicular transport of substrates in the perfused rat liver (PRL) model (Schwab et al., 1990; Geng et al., 1995; Geng et al., 1998). Interestingly, a multiple indicator dilution technique evaluated liver compartments (vascular compartment, interstitium, and accessible water space) after a bolus injection of three tracers. Sophisticated pharmacokinetic modeling was applied to describe numerous parameters. In a similar experimental rat model, we demonstrated previously how influx and efflux across membrane transporters generate the hepatocyte concentrations of two hepatobiliary substrates used in clinical practice: gadobenate dimeglumine (BOPTA) and mebrofenin (MEB) (Fig. 1A) (Bonnaventure and Pastor, 2015; Bonnaventure et al., 2019). A gamma counter is placed over a liver lobe to measure liver concentrations. Rat livers are preperfused with DTPA that distributes in sinusoids and the space of Disse to quantify extracellular concentrations (Fig. 1B). BOPTA and MEB are transported by organic anion transporting polypeptides (Oatps), multidrug resistance associated protein 2 (Mrp2), and multidrug resistance associated protein 3 (Mrp3), but MEB has a much higher hepatocyte influx clearance (CL_{in}) than BOPTA (Bonnaventure et al., 2019) (Fig. 1C). Concentrations in bile canaliculi detected by the counter are calculated from bile concentrations obtained in the common bile duct and the volume ratio of canaliculi to liver.

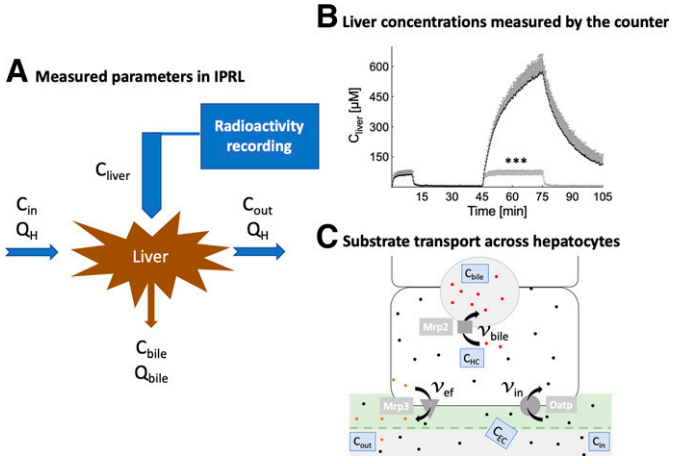

Fig. 1. (A) Perfused rat liver. Livers were perfused with a nonrecirculating system. Q_H was 30 ml/min. C_{in} values were constant during substrate perfusion: 200 µM (BOPTA) and 64 µM (MEB). C_{out} values were collected. C_{bile} and Q_{bile} were measured in the common bile duct. A gamma counter placed over a right liver lobe recorded C_{liver}. (B) Liver concentrations measured by the counter. Livers (n = 6) were perfused with KHB solution + 200 µM [^{153}Gd]DTPA, KHB, KHB + 200 µM [^{153}Gd]BOPTA, and KHB. During BOPTA perfusion, DTPA concentrations were reported (***). (C) BOPTA and MEB transport by Oatp, Mrp2, and Mrp3. C_{out} included substrates that did not enter into hepatocytes (black points) and those that entered and returned to sinusoids (brown asterisks). Substrates eliminated into bile canaliculi (red points).

The aim of this study was to compare BOPTA and MEB concentration distribution in hepatocytes, extracellular space, and bile canaliculi and calculate concentration ratios between compartments. Moreover, we analyzed the accumulation and decay profiles of hepatocyte concentrations and described new pharmacokinetic parameters to assess the activity of membrane transporters.

Materials and Methods

Animals. We perfused normal livers from male Sprague-Dawley rats (n = 12) anesthetized with pentobarbital (50 mg · kg^{-1}, i.p.). The protocol was carried out in accordance with the Swiss Guidelines for the Care and Use of Laboratory Animals and was approved by the local animal welfare committee and the veterinary office in Geneva, Switzerland.

Perfused Rat Livers. Rat livers were perfused leaving the organs in the carcass (Bonnaventure et al., 2019). The abdominal cavity was opened, and the portal vein cannulated. The hepatic artery was not perfused. The abdominal vena cava was transected, and an oxygenated Krebs-Henseleit-bicarbonate (KHB) solution was pumped into the portal vein, the solution being discarded after liver distribution via a vena cava transection. The flow rate was slowly increased over 1 minute up to 30 ml/min to prevent injury of sinusoidal cells. In a second step, the chest was opened, and a cannula was inserted through the right atrium to collect solutions flowing from hepatic veins. Finally, the abdominal inferior vena cava was ligated, allowing solutions perfused by the portal vein to be eliminated by the hepatic veins.

The perfusion system included a reservoir, a pump, a heating circulator, a bubble trap, a filter, and an oxygenator. Solutions of perfusate were equilibrated with a mixture of 95% O_2 and 5% CO_2. Livers were perfused continuously with fresh solutions using a nonrecirculating system (Fig. 1A). The common bile duct was cannulated with a PE10 catheter, and bile samples were collected every 5 minutes to measure bile flow rates (Q_{bile}, µl/min per liver) and substrate concentrations (C_{bile}, µM). Samples were collected from hepatic veins every 5 minutes [concentration in hepatic veins (C_{out}), µM].

An adequate viability of livers was assessed by a steady portal pressure below 12 mmHg during the entire protocol. Moreover, MEB bile flow rates remained steady during the entire protocol. We previously reported that a flow rate of 30 ml/min per liver maintains normal liver O_2 consumption (Pastor et al., 1998).

Perfusion of Substrates. Rat livers were perfused with either DTPA (Magnevist; Bayer imaging) and BOPTA (MultiHance; Bracco Imaging) or Technescan DTPA (DTPA, b.e.imaging GmbH, Schwyz, Switzerland) and MEB (Choletec; Bracco Imaging). DTPA distributes within sinusoids and interstitium. DTPA does not enter into hepatocytes by Oatps and does not diffuse into hepatocytes across the sinusoidal membrane because no DTPA is measured in bile. BOPTA and MEB distribute in the extracellular space before being transported into hepatocytes and bile canaliculi or back into sinusoids. BOPTA and MEB are not metabolized in hepatocytes. Magnevist and MultiHance are magnetic resonance contrast agents, whereas Technescan DTPA and Choletec are single photon emission computed tomography tracers used in clinical imaging. In this article, we use substrates as a general terminology. BOPTA and MEB are transported inside hepatocytes across the sinusoidal membranes by the Oatp transporters (Fig. 1C) (Planchamp et al., 2004; Ghibellini et al., 2008). The uptake is energy dependent but was not well described in the literature. Once inside hepatocytes, BOPTA and MEB accumulate according to their transport by Mrp2 and Mrp3, which efflux the substrates into bile canaliculi and back into sinusoids, respectively (Planchamp et al., 2007; Ghibellini et al., 2008). These transports are ATP dependent.

DTPA and BOPTA labeled with ^{153}Gd were obtained by adding $^{153}GdCl_3$ (1 MBq/ml) to the commercially available (0.5 M) solutions of DTPA and BOPTA.

Then, [^{153}Gd]DTPA and [^{153}Gd]BOPTA were diluted in the KHB solution to obtain a 200 μM concentration. Normal livers (n = 6) were successively perfused with 200 μM [^{153}Gd]DTPA (10 minutes), KHB solution (35 minutes), 200 μM [^{153}Gd]BOPTA (45–75 minutes, perfusion or accumulation period), and KHB solution (75–105 minutes, rinse or decay period).

Additionally, six normal livers were perfused with DTPA and MEB. DTPA and MEB (25 mg) were labeled with ^{99m}Tc (7 and 11 MBq, respectively). [^{99m}Tc]DTPA and [^{99m}Tc]MEB were diluted to obtain a 64 μM concentration. Livers were perfused with [^{99m}Tc]DTPA (10 minutes), KHB solution (35 minutes), [^{99m}Tc]MEB (45–75 minutes, accumulation period), and KHB solution (75–105 minutes, decay period). The protocol period lasted 105 minutes for each group. We chose to label DTPA and the hepatobiliary substrate with the same tracer. Indeed, labeling with ^{99m}Tc requires tethering a bulky chelating group that might modify the substrate behavior. The presence of free ligand or free metal in solutions with ^{153}Gd-labeled substrates was determined by complexometry at pH 5.8, with xylenol orange as indicator (Schmitz et al., 1996). The mass balance was calculated for each liver to verify the accuracy of the data. We perfused 180 μmol (200 μM at 30 ml/min during 30 minutes) of BOPTA and recovered this amount in hepatic veins, liver, and bile. For example, in a normal liver perfused with 180 μmol, we recovered 163.35 μmol in hepatic veins, 14.24 μmol in bile, and 1.14 μmol in the liver at the end of the protocol. The total amount was 178.73 μmol. Livers with a recovery less than 178 μmol were eliminated.

Substrate Concentrations in Liver Compartments. To quantify substrate concentrations in liver compartments (μM), a gamma counter that collects count rates every 20 seconds was placed 1 cm above the right liver lobe (Fig. 1A). The counter measured the radioactivity in a region of interest that was identical in each liver. To transform count rates into substrate concentrations, the total liver radioactivity was measured by an activimeter at the end of each experiment and related to the last count rates. DTPA, BOPTA, and MEB concentrations (μM) in the common bile duct and hepatic veins were measured every 5 minutes with a gamma counter. We considered that 1 g of liver was close to 1 ml. All concentrations measured in solutions or livers ranged within standard values, but bile samples had to be diluted. Radioactivity was corrected for decay.

Calculation of Hepatocyte Concentrations. The gamma counter delineated a region of interest from which all count rates originating from the extracellular, bile canaliculi, and hepatocyte compartments were divided by the liver weight to obtain liver concentration (C_{liver}, μM). To calculate hepatocyte concentrations, BOPTA liver concentrations were corrected for concentrations in the extracellular space (C_{EC}) and bile canaliculi (C_{BC}). BOPTA extracellular concentrations cannot be measured because the substrate rapidly enters into hepatocytes (<2 minutes). Therefore, BOPTA C_{EC} was estimated by DTPA C_{liver} because the substrate distributes only into the extracellular space. DTPA and BOPTA have close molecular structures and are labeled with the same tracer. The concentrations were constant during the 10-minute perfusion. From BOPTA $C_{liver} - C_{EC}$, we subtracted the concentrations originating from bile canaliculi. Assuming that the in situ concentrations of bile canaliculi were similar to those measured in the common bile duct (C_{bile}, μM), the concentrations measured by the counter (C_{BC}, μM) are defined by 0.0043 • C_{bile}. The volume ratio of bile canaliculi to liver (0.0043) was previously estimated by Blouin et al. (1977) in rat liver biopsy. Finally, hepatocyte concentrations ($C_{HC78\%}$) detected by the counter were $C_{liver} - C_{EC} - 0.0043 \bullet C_{bile}$. Assuming that the volume ratio of hepatocytes to liver was 0.78 (Blouin et al., 1977), to obtain the in situ concentrations in hepatocytes ($C_{HC100\%}$), we multiplied $C_{HC78\%}$ by 100/78.

Transfer Rates and Clearances Between Compartments. The substrate removal rate from sinusoids over time (v, nmol/min) were measured by $Q_H \bullet (C_{in} - C_{out})$, where Q_H is the constant liver perfusate flow rate (30 ml/min), C_{in} (μM) is the constant portal concentration, and C_{out} (μM) is the concentration in hepatic veins. The unbound fraction in solutions was 1 because no protein was added. CL_H (ml/min) was the ratio of v and C_{in} during the last minute of perfusion. The BOPTA and MEB extraction ratio (ER) was $(C_{in} - C_{out})/C_{in}$.

The biliary excretion rate (v_{bile}, nmol/min) was $C_{bile} \bullet Q_{bile}$, where C_{bile} (μM) was the concentration in the common bile duct and Q_{bile} was the bile flow rate (μl/min per liver weight). The clearance from hepatocytes to bile canaliculi (CL_{bile}, ml/min) was the slope of the linear regression between v_{bile} (y-axis) and C_{HC} (x-axis) measured during the accumulation and decay periods.

During the rinse period, substrate C_{out} values were substrate that effluxed from hepatocytes, the portal vein being perfused with a KHB solution (Fig. 1C). Basolateral efflux out of hepatocytes (v_{ef} in nmol/min) was determined as $C_{out} \bullet Q_H$, and basolateral efflux clearance (CL_{ef}, ml/min) was the slope of linear regression between v_{ef} (y-axis) and C_{HC} (x-axis).

During the perfusion period, C_{out} measured both substrate that returned into sinusoids after previous entry into hepatocytes and substrate that did not enter into hepatocytes. To measure concentrations that efflux from hepatocytes (C_{ef}) during this period, we used the equation $(C_{HC} \bullet CL_{ef})/Q_H$. During the last minute of perfusion, the hepatocyte influx rate of substrates (v_{in}) was defined by $[C_{in} - (C_{out} - C_{ef})] \bullet Q_H$ and was higher than the removal rate from sinusoids (v) defined by $(C_{in} - C_{out}) \bullet Q_H$. Hepatocyte influx clearance CL_{in} (ml/min) was v_{in}/C_{in}.

Accumulation Profile of Substrates in Hepatocytes. Hepatocyte accumulation was best described by nonlinear regression (or hinge function) obtained from GraphPad Prism version 8 (GraphPad Software, La Jolla, CA) (Motulsky, 2021b) (Fig. 3C). The equation describes a first line L_1 that characterizes BOPTA and MEB influx into hepatocytes. A second line L_2 is described when BOPTA and MEB efflux from hepatocytes decreases the accumulation rates of substrate. The equation precisely calculates the time (T_0) when efflux back to sinusoids and biliary excretion affects the accumulation profile, changing the slope of L_1. The hinge function is a segmental linear regression with a gentle curve connecting L_1 and L_2. This gentle connection is linked to a slow increase of $v_{bile} + v_{ef}$ (Fig. 3, A and B).

Concentration Ratios Between Compartments. In in vivo studies, only liver-to-plasma concentration ratios are available. However, concentrations facing the basolateral membrane of hepatocytes where Oatps reside are the extracellular concentrations because the space of Disse intertwines between sinusoids and the basolateral membrane. Thus, the hepatocyte-to-extracellular concentration ratio ($R_{HC/EC}$) characterizes influx into hepatocytes. $R_{HC/EC}$ was measured at T_0 before the time when substrate cellular efflux began to affect C_{HC}. The bile-to-hepatocyte concentration ratio ($R_{bile/HC}$) was the slope of the relationship between C_{bile} (y-axis) and C_{HC} (x-axis) during the accumulation and rinse periods. $R_{bile/HC}$ is independent of substrate influx into hepatocytes. The hepatic vein–to-hepatocyte ratio ($R_{HV/HC}$) was the slope of the relationship between C_{out} (y-axis) and C_{HC} (x-axis) during the rinse period. $R_{HV/HC}$ estimates Mrp3 transport and is independent of substrate influx into hepatocytes. Finally, the bile-to-extracellular concentration ratio ($R_{bile/EC}$) assessed the ability of transporters to concentrate substrates from the extracellular space to the bile compartment. $R_{bile/EC}$ was measured at the end of the perfusion period when bile concentrations were maximal. Hepatocyte concentrations used in the ratios were in situ concentrations.

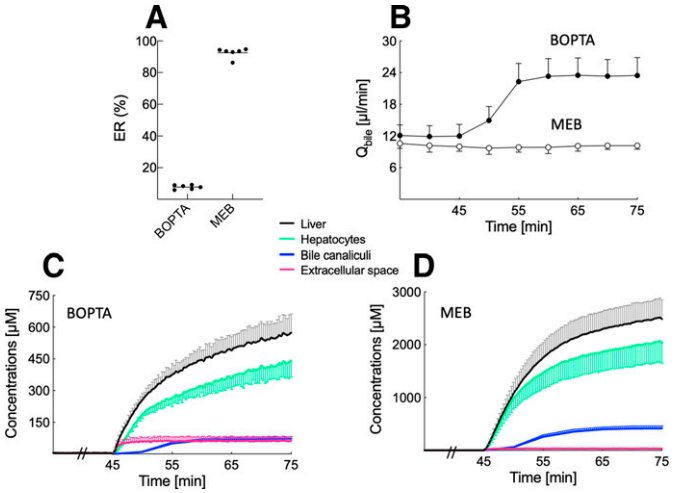

Fig. 2. (A) BOPTA and MEB liver extraction ratios. (B) Q_{bile} measured during BOPTA and MEB perfusion. (C) Compartmental distribution of BOPTA in normal livers (n = 6) perfused with KHB solution + 200 μM [^{153}Gd]BOPTA (45–75 minutes) (D) Compartmental distribution of MEB in normal livers (n = 6) perfused with KHB + 64 μM [^{99m}Tc]MEB (45–75 minutes). Liver concentrations (black symbols) were measured by a gamma counter. Concentrations in extracellular compartment (red symbols) were measured during the previous DTPA perfusion. Concentrations that originate from the bile canaliculi (blue symbols) and from hepatocyte volume (green symbols) were calculated.

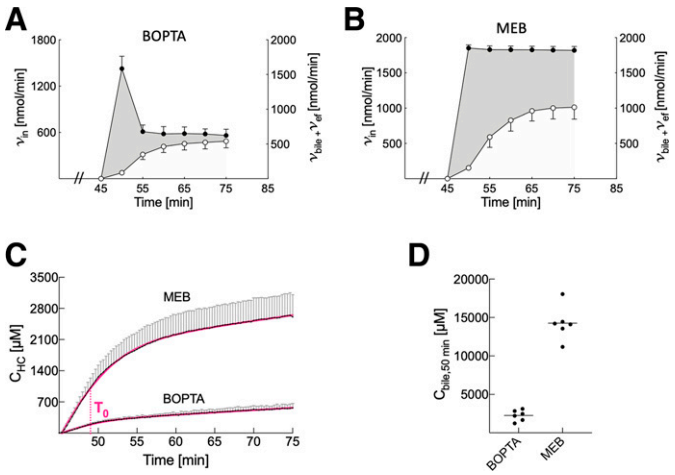

Fig. 3. BOPTA (A) and MEB (B) hepatocyte influx rate (v_{in}, left *y*-axis, black circles) and bile excretion rate (v_{bile}) plus basolateral efflux rate (v_{ef}) (right *y*-axis, open circles) during accumulation period (45–75 minutes). Normal livers ($n = 12$) were perfused with KHB solution + 200 μM [^{153}Gd]BOPTA or KHB + 64 μM [^{99m}Tc]MEB. Difference between v_{in} and $v_{bile} + v_{ef}$ (gray area). (C) Accumulation of BOPTA and MEB hepatocyte concentrations (from 45 to 75 minutes of the experimental protocol). Accumulation was best described by a hinge function (red curve) defined by two lines with a gentle connection between them that intersected at T_0 defined as the time when cellular excretion affects hepatocyte concentrations. (D) Bile concentrations measured 5 minutes after the start of substrate perfusion (time 50 minutes of the experimental protocol).

Decay Profile of Hepatocyte Concentrations. During the decay period, we compared one-phase and two-phase decay using Akaike's information criterion (GraphPad Prism version 8). The plateau was constrained to 0 because BOPTA and MEB exit from hepatocytes. Data were best described by a two-phase decay (Motulsky, 2021a), consisting of two components working simultaneously and defined by fast and slow elimination rate constants of hepatocyte concentration, $k_{fast,HC}$ and $k_{slow,HC}$ (min^{-1}), with initial Y values ($Y_{0,fast}$ and $Y_{0,slow}$).

Statistics. Data represent means ± S.D. Parameters from livers perfused with BOPTA and MEB were compared with a Mann-Whitney test (GraphPad Prism version 8).

Results

Basic Parameters During the Accumulation Period. At the end of the accumulation period, the liver ER of MEB was 0.93 ± 0.03, whereas BOPTA ER was 0.08 ± 0.01 ($P = 0.002$; Fig. 2A). MEB C_{out} was 5 ± 2 μM when C_{in} was 64 μM, whereas BOPTA C_{out} (185 ± 3 μM) remained slightly lower than the perfused concentrations (200 μM; Table 1). BOPTA is a choleretic substrate (bile flow rates increased to a plateau during substrate perfusion), whereas MEB is not choleretic (Fig. 2B).

BOPTA and MEB Accumulation in Liver Compartments. BOPTA and MEB accumulated in liver compartments during the perfusion period. Distribution in the extracellular compartment was steady over the period (Fig. 2, C and D). MEB C_{EC} was low (~1% of liver concentrations) and therefore did not interfere appreciably with liver concentrations (Table 1), whereas BOPTA C_{EC} (62 ± 20 μM) contributed to ~10% of liver concentrations throughout the period. C_{BC} contributed to liver concentrations for both substrates. At the end of the perfusion period, C_{BC} values were 72 ± 9 μM (BOPTA) and 417 ± 49 μM (MEB) ($P = 0.002$; Table 1).

Accumulation Profile of BOPTA and MEB Concentrations in Hepatocytes. Influx rates (v_{in}) increased rapidly 5 minutes after the start of perfusion for both substrates (Fig. 3, A and B). High v_{in} was maintained during the perfusion period for MEB, which has a liver extraction of 0.93, but not for BOPTA, which has a low (0.08) liver extraction. The hepatocyte accumulation profiles relied on the concomitant influx (v_{in}) and efflux ($v_{bile} + v_{ef}$) rates. Steady state was not reached at the end of the substrate perfusion, and v_{in} remained higher than $v_{bile} + v_{ef}$ for both substrates (Table 1). At the end of the perfusion, CL_{in} was 2.8 ± 0.4 ml/min (BOPTA) and 28.1 ± 0.8 ml/min (MEB; $P = 0.002$). CL_H was lower than CL_{in} for both substrates because v_{in} was calculated by $[C_{in} - (C_{out} - C_{ef})] \bullet Q_H$ (Table 1).

BOPTA and MEB hepatocyte accumulation was best described by a hinge function (Fig. 3C). This function defined a first line L_1 for time below T_0 and a second line L_2 for time higher than T_0 while ensuring that the two lines intersected at T_0. The first and high accumulation phase lasted less than 5 minutes. T_0 occurred at 4.3 ± 1.0 minutes (BOPTA) and 3.9 ± 1.4 minutes (MEB) after the start of substrate perfusion ($P = 0.54$; Table 2). Before T_0, the L_1 slope characterizes BOPTA and MEB influx by Oatps: the slopes were 70 ± 15 μM/min (BOPTA) and 425 ± 82 μM/min (MEB; $P = 0.004$). After T_0, the accumulation rates decreased, and the L_2 slopes were much lower than L_1 slopes (BOPTA: 10 ± 3 μM/min; MEB: 24 ± 6 μM/min). Concomitant entry and efflux from hepatocytes were responsible for the low L_2 slopes. The hinge from L_1 to L_2 was smooth. A steady increase in biliary excretion and basolateral efflux rates explained the smoothness (Fig. 3C). Five minutes after the start of substrate perfusion, bile concentrations were higher than 2,000 μM in both groups (Fig. 3D).

Concentration Ratios Between Liver Compartments. The MEB concentration ratio between hepatocytes and extracellular space ($R_{HC/EC}$) at T_0 was higher than BOPTA $R_{HC/EC}$ (33 ± 19 versus 4 ± 2, respectively) (Table 1; $P = 0.002$). The bile-to-hepatocyte concentration ratio ($R_{bile/HC}$) was slightly higher for MEB (45 ± 12) than BOPTA (31 ± 6; $P = 0.03$). In contrast, the concentration ratio between sinusoids and hepatocytes ($R_{HV/HC}$) was more than an order of magnitude higher for BOPTA than MEB. Finally, the maximal concentration ratio between bile and extracellular space ($R_{bile/EC}$), which was measured at the end of the perfusion period, was approximately an order of magnitude higher for MEB than BOPTA (Table 1).

Decay Profile of Hepatocyte Concentrations and Efflux Clearance Values. During the decay period, hepatocyte concentrations were best described by a two-phase decay (Fig. 4A), consisting of two components working simultaneously and defined by rate constants $k_{fast,HC}$ and $k_{slow,HC}$ (min^{-1}) with initial Y values ($Y_{0,fast}$ and $Y_{0,slow}$). BOPTA $k_{fast,HC}$ (0.25 ± 0.19 min^{-1}) and MEB $k_{fast,HC}$ (0.21 ± 0.02 min^{-1}) were not significantly different ($P = 0.39$). BOPTA $k_{slow,HC}$ (0.044 ± 0.007 min^{-1}) was higher than MEB $k_{slow,HC}$ (0.016 ± 0.004 min^{-1}; $P = 0.004$).

BOPTA and MEB CL_{bile} was determined by the slope of the linear regression between v_{bile} (*y*-axis) and C_{HC} (*x*-axis) (Fig. 5, A and B). BOPTA CL_{bile} [0.89 ± 0.25 ml of hepatocytes (ml_{HC})/min or ml_{HC}/min] was higher than MEB CL_{bile} (0.47 ± 0.15 ml_{HC}/min; $P = 0.009$). For both substrates, CL_{bile} measured during the rinse and perfusion periods was similar. BOPTA and MEB CL_{ef} was measured during the rinse period by the slope of the linear regression between v_{ef} (*y*-axis) and C_{HC} (*x*-axis) (Fig. 5, C and D). BOPTA CL_{ef} (0.18 ± 0.03 ml_{HC}/min was significantly higher than MEB CL_{ef} (0.01 ± 0.01 ml_{HC}/min; $P = 0.002$).

Discussion

The PRL includes a gamma counter that mimics an imaging system to measure liver concentrations. With this technique, we are able to differentiate in situ concentrations that govern transporter function from concentrations detected by the counter. Thus, at the end of the accumulation period, MEB C_{bile} values are 97,017 ± 11,289 μM, whereas the C_{BC} values are 417 ± 49 μM or $C_{bile} \bullet 0.0043$. The extracellular concentrations facing Oatps are measured by DTPA preperfusion. Hepatocyte concentrations measured by the counter are calculated by $C_{liver} - C_{EC} - C_{bile} \bullet 0.0043$. A correction is applied to obtain the in situ C_{HC}, which is the concentration facing Mrp2 and Mrp3. The liver ER influences the compartmental

TABLE 1

Concentrations, transfer rates, and clearance values

	Imaging substrates		
	BOPTA	MEB	*P*
Concentrations (μM)			
End of perfusion period			
C_{in}	200	64	
C_{out}	185 ± 3	5 ± 2	0.002
C_{liver}	574 ± 88	2,486 ± 362	0.002
C_{EC}	62 ± 20	32 ± 7	0.004
$C_{HC78\%}$	441 ± 78	2,036 ± 389	0.002
$C_{HC100\%}$	566 ± 99	2,610 ± 498	0.002
C_{BC}	72 ± 9	417 ± 49	0.002
C_{bile}	16,791 ± 2,085	97,017 ± 11,289	0.002
Transfer rates (nmol/min)			
End of perfusion period			
v	464 ± 80	1,797 ± 61	0.002
v_{in}	561 ± 81	1,819 ± 54	0.002
v_{bile} (nmol/min)	390 ± 84	990 ± 166	0.002
v_{ef}	97 ± 7	22 ± 8	0.002
Clearance parameters			
End of perfusion period			
CL_H (ml_{KHB}/min)	2.3 ± 0.4	27.8 ± 0.9	0.002
CL_{in} (ml_{KHB}/min)	2.8 ± 0.4	28.1 ± 0.8	0.002
Perfusion and rinse periods			
CL_{bile} (ml_{HC}/min)	0.89 ± 0.25	0.47 ± 0.15	0.009
Rinse period			
CL_{ef} (ml_{HC}/min)	0.18 ± 0.03	0.01 ± 0.01	0.002
CL_{bile} + CL_{ef} (mlHC/min)	1.1 ± 0.3	0.5 ± 0.1	0.004
Concentration ratios			
$R_{HC/EC}$	4 ± 2	33 ± 19	0.002
$R_{bile/HC}$	31 ± 6	45 ± 12	0.03
$R_{HV/HC}$	0.006 ± 0.001	0.0003 ± 0.0001	0.002
$R_{bile/EC}$	299 ± 111	3218 ± 1109	0.002

$C_{HC100\%}$ is $C_{HC78\%}$ multiplied by 100/78. Substrate removal rate from sinusoids (v), hepatocyte influx rate (v_{in}), bile excretion rate (v_{bile}), and efflux rate back into sinusoids (v_{ef}). Hepatocyte-to-extracellular concentration ratio ($R_{HC/EC}$) were measured at T_0 in the absence of hepatocyte efflux. Bile-to-hepatocyte concentration ratio ($R_{bile/HC}$) was the slope of the relationship between C_{HC} (*x*-axis) and C_{bile} (*y*-axis) during the perfusion and rinse periods. Hepatic vein–to-hepatocyte concentration ratio ($R_{HV/HC}$) was the slope of the relationship between C_{HC} (*x*-axis) and C_{ef} (*y*-axis) during the rinse period. Bile-to-extracellular concentration ratio ($R_{bile/EC}$) was the maximal ability of transporters to concentrate substrates from the EC to bile compartment at the end of the perfusion period. CL_H and CL_{in} were expressed in ml of Krebs-Henseleit Bicarbonate (KHB) solution/min (ml_{KHB}/min). CL_{ef} and CL_{bile} were expressed in ml of hepatocytes (HC)/min (ml_{HC}/min).

distribution of substrates. Extracellular concentrations do not contribute appreciably to MEB liver concentrations, which rely mainly on hepatocytes and bile canaliculi. In contrast, all three compartments contribute to BOPTA liver concentrations.

Besides compartmental distribution, the PRL assesses BOPTA and MEB transport across hepatocytes by calculating concentration ratios between compartments. BOPTA and MEB Oatp transport was quantified by several parameters such as the hepatocyte-to-extracellular concentration ratio ($R_{HC/EC}$) at T_0, before efflux out of cells affects C_{HC}. $R_{HC/EC}$ was higher than the commonly available liver-to–portal vein ratio because C_{EC} concentrations were lower than portal vein concentrations. The value of T_0 (~4 minutes) was similar for BOPTA and MEB. Typically, the time when the substrate efflux out starts to affect C_{HC} is independent of the liver extraction ratio. Five minutes after the start of the perfusion, BOPTA and MEB bile concentrations were measurable. Another way to assess BOPTA and MEB influx into hepatocytes is to compare the L_1 slope given by the equation that describes the accumulation profile. Similar to $R_{HC/EC}$, the MEB L_1 slope was much higher than the BOPTA L_1 slope, as anticipated by the high ER of MEB. When time is greater than T_0, the hepatocyte accumulation rate (L_2 slope) is much lower than the L_1 slope because BOPTA and MEB efflux out of cells. CL_H and CL_{in} were quantified at the end of the perfusion period. At that time, steady state was not reached, and v_{in} remained higher than v_{bile} + v_{ef}. To calculate v_{in}, we must estimate C_{ef} during the perfusion period. We assume that CL_{ef} is similar during the perfusion and rinse periods. CL_H and CL_{in} were much higher for MEB than BOPTA.

To quantify BOPTA and MEB Mrp2 transport, we measured the bile-to-hepatocyte concentration ratio ($R_{bile/HC}$), which is independent of substrate entry into hepatocytes. $R_{bile/HC}$ is the slope of the relationship between C_{bile} and C_{HC} and was quantified during the entire protocol. The ratio was slightly higher for MEB than BOPTA. However, BOPTA transport by Mrp2 is associated with water transport (choleresis), whereas MEB is not. The increased water content in bile canaliculi decreased BOPTA concentrations and underestimated its transport by Mrp2. This water permeability linked to Mrp2 results from the trafficking and insertion of aquaporin-8–containing vesicles into the canalicular membrane (Marinelli et al., 2019; Marrone et al., 2021). The BOPTA-induced choleresis is concentration dependent and is not observed in livers lacking Mrp2 (Millet et al., 2011). Similar results were published with benzylpenicillin (Ito et al., 2004). In contrast, BOPTA and MEB CL_{bile} (ml_{HC}/min) was independent of bile volume. CL_{bile} was calculated as the slope of the linear regression between v_{bile} and C_{HC}. BOPTA CL_{bile} was approximately two times higher than MEB CL_{bile}.

The BOPTA and MEB hepatic vein–to-hepatocyte concentration ratio ($R_{HV/HC}$) was calculated during the rinse period. The ratio is independent of substrate influx. $R_{HV/HC}$ is much lower than $R_{bile/HC}$ for both substrates, and MEB $R_{HV/HC}$ is more than 10 times lower than BOPTA $R_{HV/HC}$. BOPTA and MEB CL_{ef} (ml_{HC}/min), a measure of Mrp3 transport, was estimated from the slope of the linear regression between v_{ef} and C_{HC}. MEB CL_{ef} was more than 10 times lower than BOPTA CL_{ef}. Thus, MEB is not extensively transported by Mrp3. In contrast, BOPTA efflux by Mrp3 back to sinusoids contributes significantly to the decrease

TABLE 2

BOPTA and MEB hepatocyte accumulation and decay

	Imaging substrate		
	BOPTA	MEB	*P*
Accumulation			
T_0 (min)	4.3 ± 1.0	3.9 ± 1.4	0.54
L_1 slope (μM/min)	70 ± 15	425 ± 82	0.004
L_2 slope (μM/min)	10 ± 3	24 ± 6	0.004
Decay			
Y_0 (μM)	588 ± 89	2731 ± 499	0.002
$Y_{0,fast}$ (μM)	327 ± 61	1723 ± 328	0.004
$k_{fast,HC}$ (min^{-1})	0.25 ± 0.19	0.21 ± 0.02	0.39
$T_{1/2fast}$ (min)	3.2 ± 1.6	3.3 ± 0.3	0.66
$Y_{0,slow}$ (μM)	235 ± 55	1008 ± 308	0.004
$k_{slow,HC}$ (min^{-1})	0.044 ± 0.007	0.016 ± 0.004	0.004
$T_{1/2slow}$ (min)	16 ± 3	48 ± 17	0.004
Rate constant ratio	6.4 ± 3.4	14.5 ± 4.5	0.02

Hepatocyte accumulation was best described by a hinge function that included a first line L_1 for time below T_0 and a second line L_2 for time higher than T_0. T_0 was the time when the two lines would intersect if there were no curve connecting them. Before T_0, L_1 slope characterized BOPTA and MEB influx by Oatps. After T_0, accumulation rates decreased due to concomitant entry and efflux from hepatocytes. During decay, hepatocyte concentrations were best described with a two-phase decay model. The model was the sum of two components working simultaneously and defined by rate constants $k_{fast,HC}$ and $k_{slow,HC}$ and starting Y values ($Y_{0,fast}$ and $Y_{0,slow}$). For each liver, Y_0 is $Y_{0,fast}$ + $Y_{0,slow}$.

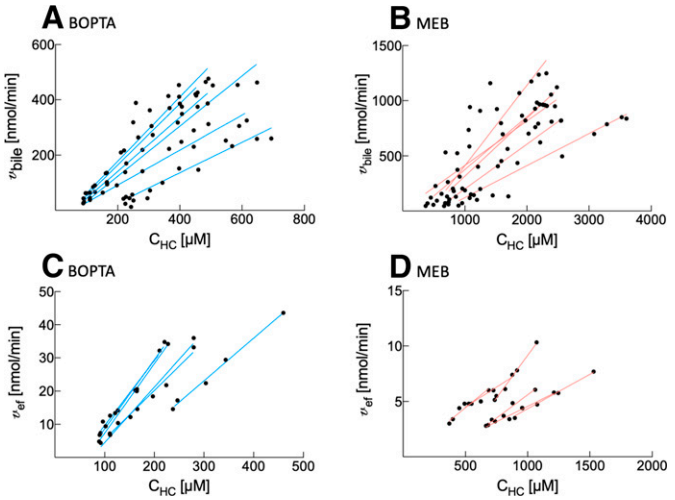

Fig. 5. BOPTA (A) and MEB (B) CL_{bile} (ml_{HC}/min). CL_{bile} was the slope of the linear regression between v_{bile} and C_{HC} during the accumulation and decay periods. BOPTA (C) and MEB (D) CL_{ef} (ml_{HC}/min). CL_{ef} was the slope of linear regression between v_{ef} and C_{HC} during the rinse period.

in hepatocyte concentrations. Such results have been previously published (Ghibellini et al., 2008; Bonnaventure et al., 2019).

BOPTA and MEB Mrp3 and Mrp2 transport was also quantified by a two-phase decay with a plateau constrained to 0 because BOPTA and MEB have to leave hepatocytes. Physiologically, this may represent two groups of hepatocytes (with low and high concentrations) working simultaneously and defined by rate constants $k_{fast,HC}$ and $k_{slow,HC}$ (min^{-1}) (Motulsky, 2021a). We hypothesize that hepatocytes with high concentrations might be located in the perivenous areas where Oatp expression is maximal (Reichel et al., 1999; Tachikawa et al., 2018) (Akanuma et al., 2019). Interestingly, $k_{fast,HC}$ was similar for BOPTA and MEB. However, questions remain on the interpretation of these parameters related to the decrease in hepatocyte concentrations.

The PRL is an interesting model to quantify the compartmental distribution of substrates, the concentration ratios between liver compartments, and hepatocyte influx and efflux clearance values. We clearly show that MEB has a higher Oatp-mediated CL_{in} than BOPTA but that CL_{bile}-mediated by Mrp2 is higher for BOPTA than MEB. MEB is not transported appreciably by Mrp3, whereas BOPTA transport back to sinusoids contributes to the decrease in hepatocyte concentrations. Besides the classic concept of plasma concentration decay, cellular concentrations are important to investigate when transporter-dependent drugs target hepatocytes. Low concentrations on cellular targets may impair therapeutic effects, whereas excessive hepatocyte concentrations may induce cellular toxicity. We show that the interpretation of hepatocyte concentrations is complex because it relies on three independent processes involved in hepatobiliary disposition: basolateral uptake, basolateral efflux, and biliary excretion, which are dependent on membrane transporters. With this in situ model, we showed previously how rifampicin modified BOPTA and MEB hepatocyte concentrations by modifying clearance parameters (Bonnaventure et al., 2019).

The concentration ratios we quantify are different from the classic liver-to-plasma concentration ratio (Riccardi et al., 2017; Riede et al., 2017; Guo et al., 2018). We used the hepatocyte-to–extracellular space ratio because concentrations facing the basolateral membrane of hepatocytes, where Oatps reside, are the extracellular concentrations. The space of Disse intertwines between sinusoids and the basolateral membrane. Moreover, the time of measurement is important, especially for influx parameters that are measured before T_0 (defined as the time when substrate efflux affects hepatocyte concentrations).

In the PRL model, the experiments are simplified. BOPTA and MEB are free to enter into hepatocytes because perfused solutions do not contain protein. The hepatic artery is not perfused. BOPTA and MEB are not metabolized in hepatocytes. Both substrates have a low protein binding in cells and bile that do not interfere with the concentrations and the transfer rates measured (Cavagna et al., 1997; Ghibellini et al., 2008). An important assumption is that the region of interest measured by the counter is representative of the entire liver. Because our main interest was to measure hepatocyte concentrations, we did not determine the volume of distribution of hepatocytes and bile canaliculi. We used values published in the literature. It is clear that changing these volume ratios modifies the pharmacokinetic parameters. If the volume of hepatocytes to liver is lower, $C_{HC100\%}$ would increase, whereas CL_{bile} and CL_{ef} would decrease.

In conclusion, our ex vivo model quantifies substrate compartmental distribution and transport across hepatocyte membranes and provides an additional understanding of drug distribution in the liver.

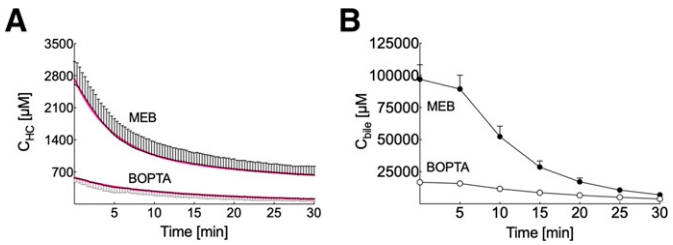

Fig. 4. (A) BOPTA and MEB hepatocyte concentrations during the decay period (75–105 minutes) when livers were perfused with Krebs-Henseleit bicarbonate solution (rinse period). The decline in concentrations was best described by a two-phase decay (red curves). (B) BOPTA and MEB bile concentration decay.

Authorship Contributions

Participated in research design: Pastor.
Conducted experiments: Pastor.
Contributed new reagents or analytic tools: Pastor, Brouwer.
Performed data analysis: Pastor, Brouwer.
Wrote or contributed to the writing of the manuscript: Pastor, Brouwer.

References

Akanuma SI, Kida R, Tsuchiyama A, Tachikawa M, Kubo Y, and Hosoya KI (2019) Organic anion-transporting polypeptide 1a4-mediated heterogeneous distribution of sulforhodamine-101 in rat hepatic lobules. *Drug Metab Pharmacokinet* **34**:239–246.

Ali I, Slizgi JR, Kaullen JD, Ivanovic M, Niemi M, Stewart PW, Barritt 4th AS, and Brouwer KLR (2018) Transporter-mediated alterations in patients with NASH increase systemic and hepatic exposure to an OATP and MRP2 substrate. *Clin Pharmacol Ther* **104**:749–756.

Beaudoin JJ, Brock WJ, Watkins PB, and Brouwer KLR (2021) Quantitative systems toxicology modeling predicts that reduced biliary efflux contributes to Tolvaptan hepatotoxicity. *Clin Pharmacol Ther* **109**:433–442.

Benet LZ, Liu S, and Wolfe AR (2018) The universally unrecognized assumption in predicting drug clearance and organ extraction ratio. *Clin Pharmacol Ther* **103**:521–525.

Billington S, Shoner S, Lee S, Clark-Snustad K, Pennington M, Lewis D, Muzi M, Rene S, Lee J, Nguyen TB et al. (2019) PET imaging of [(11)C]rosuvastatin hepatic concentrations and hepatobiliary transport in humans in the absence and presence of cyclosporine A. *Clin Pharmacol Ther* **106**:1056–1066.

Blouin A, Bolender RP, and Weibel ER (1977) Distribution of organelles and membranes between hepatocytes and nonhepatocytes in the rat liver parenchyma. A stereological study. *J Cell Biol* **72**:441–455.

Bonnaventure P, Cusin F, and Pastor CM (2019) Hepatocyte concentrations of imaging compounds associated with transporter inhibition: evidence in perfused rat livers. *Drug Metab Dispos* **47**:412–418.

Bonnaventure P and Pastor CM (2015) Quantification of drug transport function across the multiple resistance-associated protein 2 (Mrp2) in rat livers. *Int J Mol Sci* **16**:135–147.

Cavagna FM, Maggioni F, Castelli PM, Daprà M, Imperatori LG, Lorusso V, and Jenkins BG (1997) Gadolinium chelates with weak binding to serum proteins. A new class of high-efficiency, general purpose contrast agents for magnetic resonance imaging. *Invest Radiol* **32**:780–796.

De Lombaerde S, Neyt S, Vanhove C, and De Vos F (2019) In vivo measurement of hepatic drug transporter inhibition with radiolabeled bile acids. *Methods Mol Biol* **1981**:87–98.

Geng W, Schwab AJ, Horie T, Goresky CA, and Pang KS (1998) Hepatic uptake of bromosulfophthalein-glutathione in perfused Eisai hyperbilirubinemic mutant rat liver: a multiple-indicator dilution study. *J Pharmacol Exp Ther* **284**:480–492.

Geng WP, Schwab AJ, Goresky CA, and Pang KS (1995) Carrier-mediated uptake and excretion of bromosulfophthalein-glutathione in perfused rat liver: a multiple indicator dilution study. *Hepatology* **22**:1188–1207.

Ghibellini G, Leslie EM, Pollack GM, and Brouwer KL (2008) Use of Tc-99m mebrofenin as a clinical probe to assess altered hepatobiliary transport: integration of in vitro, pharmacokinetic modeling, and simulation studies. *Pharm Res* **25**:1851–1860.

Guo Y, Chu X, Parrott NJ, Brouwer KLR, Hsu V, Nagar S, Matsson P, Sharma P, Snoeys J, Sugiyama Y et al. (2018) Advancing predictions of tissue and intracellular drug concentrations using in vitro, imaging and PBPK modeling approaches. *Clin Pharmacol Ther* **104**:865–889.

Hernández Lozano I, Karch R, Bauer M, Blaickner M, Matsuda A, Wulkersdorfer B, Hacker M, Zeitlinger M, and Langer O (2019) Towards improved pharmacokinetic models for the analysis of transporter-mediated hepatic disposition of drug molecules with positron emission tomography. *AAPS J* **21**:61.

Hernández Lozano I and Langer O (2020) Use of imaging to assess the activity of hepatic transporters. *Expert Opin Drug Metab Toxicol* **16**:149–164.

Ito K, Koresawa T, Nakano K, and Horie T (2004) Mrp2 is involved in benzylpenicillin-induced choleresis. *Am J Physiol Gastrointest Liver Physiol* **287**:G42–G49.

Leporq B, Daire JL, Pastor CM, Deltenre P, Sempoux C, Schmidt S, and Van Beers BE (2018) Quantification of hepatic perfusion and hepatocyte function with dynamic gadoxetic acid-enhanced MRI in patients with chronic liver disease. *Clin Sci (Lond)* **132**:813–824.

Marinelli RA, Vore M, and Javitt NB (2019) Hepatic bile formation: canalicular osmolarity and paracellular and transcellular water flow. *J Pharmacol Exp Ther* **371**:713–717.

Marrone J, Danielli M, Gaspari CI, Capiglioni AM, and Marinelli RA (2021) Aquaporin gene transfer for hepatocellular cholestasis. *Biochimie* **188**:12–15.

Millet P, Moulin M, Stieger B, Daali Y, and Pastor CM (2011) How organic anions accumulate in hepatocytes lacking Mrp2: evidence in rat liver. *J Pharmacol Exp Ther* **336**:624–632.

Motulsky HJ (2021a) Equation: Two phase decay, in *GraphPad Curve Fitting Guide*, GraphPad Software, La Jolla, CA. https://www.graphpad.com/guides/prism/latest/curve-fitting/reg_exponential_decay_2phase.htm.

Motulsky HJ (2021b) Equation: Hinge function. Segmental regression lines with gentle connection, in *GraphPad Curve Fitting Guide*, GraphPad Software, La Jolla, CA. https://www.graphpad.com/guides/prism/latest/curve-fitting/reg_equation-hinge-function.htm?q=hinge+function.

Pastor CM, Morel DR, and Billiar TR (1998) Oxygen supply dependence of urea production in the isolated perfused rat liver. *Am J Respir Crit Care Med* **157**:796–802.

Pastor CM, Planchamp C, Pochon S, Lorusso V, Montet X, Mayer J, Terrier F, and Vallée JP (2003) Kinetics of gadobenate dimeglumine in isolated perfused rat liver: MR imaging evaluation. *Radiology* **229**:119–125.

Planchamp C, Gex-Fabry M, Dornier C, Quadri R, Reist M, Ivancevic MK, Vallée JP, Pochon S, Terrier F, Balant L et al. (2004) Gd-BOPTA transport into rat hepatocytes: pharmacokinetic analysis of dynamic magnetic resonance images using a hollow-fiber bioreactor. *Invest Radiol* **39**:506–515.

Planchamp C, Hadengue A, Stieger B, Bourquin J, Vonlaufen A, Frossard JL, Quadri R, Becker CD, and Pastor CM (2007) Function of both sinusoidal and canalicular transporters controls the concentration of organic anions within hepatocytes. *Mol Pharmacol* **71**:1089–1097.

Reichel C, Gao B, Van Montfoort J, Cattori V, Rahner C, Hagenbuch B, Stieger B, Kamisako T, and Meier PJ (1999) Localization and function of the organic anion-transporting polypeptide Oatp2 in rat liver. *Gastroenterology* **117**:688–695.

Riccardi K, Lin J, Li Z, Niosi M, Ryu S, Hua W, Atkinson K, Kosa RE, Litchfield J, and Di L (2017) Novel method to predict in vivo liver-to-plasma Kpuu for OATP substrates using suspension hepatocytes. *Drug Metab Dispos* **45**:576–580.

Riede J, Camenisch G, Huwyler J, and Poller B (2017) Current in vitro methods to determine hepatic Kpuu: a comparison of their usefulness and limitations. *J Pharm Sci* **106**:2805–2814.

Rostami-Hodjegan A (2018) Revisiting principles behind drug clearance and organ extraction. *Clin Pharmacol Ther* **103**:388–389.

Rowland M and Pang KS (2018) Commentary on "The universally unrecognized assumption in predicting drug clearance and organ extraction ratio". *Clin Pharmacol Ther* **103**:386–388.

Schmitz SA, Mühler A, Wagner S, and Wolf KJ (1996) Functional hepatobiliary imaging with Gd-EOB-DTPA. A comparison of magnetic resonance imaging and ^{153}Gd-EOB-DTPA scintigraphy in rats. *Invest Radiol* **31**:154–160.

Schwab AJ, Barker 3rd F, Goresky CA, and Pang KS (1990) Transfer of enalaprilat across rat liver cell membranes is barrier limited. *Am J Physiol* **258**:G461–G475.

Sourbron S (2014) A tracer-kinetic field theory for medical imaging. *IEEE Trans Med Imaging* **33**:935–946.

Tachikawa M, Sumiyoshiya Y, Saigusa D, Sasaki K, Watanabe M, Uchida Y, and Terasaki T (2018) Liver zonation index of drug transporter and metabolizing enzyme protein expressions in mouse liver acinus. *Drug Metab Dispos* **46**:610–618.

Tournier N, Stieger B, and Langer O (2018) Imaging techniques to study drug transporter function in vivo. *Pharmacol Ther* **189**:104–122.

Zhang D, Hop CECA, Patilea-Vrana G, Gampa G, Seneviratne HK, Unadkat JD, Kenny JR, Nagapudi K, Di L, Zhou L et al. (2019) Drug concentration asymmetry in tissues and plasma for small molecule-related therapeutic modalities. *Drug Metab Dispos* **47**:1122–1135.

Address correspondence to: Dr. Catherine M. Pastor, Department of Radiology, University Hospital of Geneva, Rue Gabrielle-Perret-Gentil, 4, 1205 Geneva, Switzerland. E-mail: catherine.pastor@unige.ch